ATLAS NOTE

ATLAS-CONF-2012-023

March 2, 2012

Search for supersymmetry in events with three leptons and missing transverse momentum in $\sqrt{s} = 7$ TeV pp collisions with the ATLAS detector

The ATLAS collaboration

Abstract

This document presents a search for the production of supersymmetric particles decaying into final states with three electrons or muons and missing transverse momentum. The analysis uses 2.06 fb^{-1} of $\sqrt{s} = 7$ TeV proton-proton collision data delivered by the Large Hadron Collider and recorded with the ATLAS detector. Observations are consistent with Standard Model expectations in two signal regions that are either depleted or enriched in Z-boson decays. Upper limits at 95% confidence level are set in R-parity conserved phenomenological minimal supersymmetric and simplified models for direct chargino and neutralino production. For the simplified models, degenerate lightest chargino and next-to-lightest neutralino masses up to 300 GeV are excluded for mass differences to the lightest neutralino up to 250 GeV.

1 Introduction

Supersymmetric (SUSY) extensions [1–9] of the Standard Model (SM) naturally address the gauge hierarchy problem in the SM, by postulating the existence of supersymmetric bosonic (fermionic) partners of the SM fermions (bosons). Charginos ($\tilde{\chi}_j^{\pm}$) and neutralinos ($\tilde{\chi}_i^0$) are mass eigenstates formed from the linear superposition of the SUSY partners of the electroweak gauge bosons (W, Z, γ) and of the Higgs bosons, called gauginos (winos, zinos, binos) and higgsinos. In many SUSY models, the $\tilde{\chi}_j^{\pm}$ and $\tilde{\chi}_i^0$ are among the lightest SUSY particles, or sparticles, and the $\tilde{\chi}_1^0$ is the lightest sparticle (LSP). In R-parity conserving models [10–14], the LSP is stable and sparticles are pair-produced. The production of light charginos and neutralinos can be abundant at the Large Hadron Collider (LHC). Charginos can decay via sleptons ($\tilde{\nu}\ell$), sneutrinos ($\tilde{\ell}\nu$) or W-bosons ($W^{\pm(*)}\tilde{\chi}_1^0$), and neutralinos can decay to $\tilde{\ell}\ell$, $\tilde{\nu}\nu$, or $Z^{(*)}\tilde{\chi}_1^0$. The leptonic decays of the SM gauge bosons and of the sleptons can give rise to a low-background signature with three SM leptons and sizable missing transverse momentum, the latter originating from the two undetected LSPs. Searches described in this paper are the first performed with the ATLAS detector in the final state with three leptons and missing transverse momentum. The results significantly extend the current mass limits on charginos and neutralinos LEP [15–19].

This document focuses on the associated production and leptonic decays of charginos and neutralinos. Here, leptons only comprise electrons and muons ($\ell = e, \mu$), including those from τ decays. The analysis is based on $2.06\,\text{fb}^{-1}$ of proton-proton collision data at a center-of-mass energy $\sqrt{s} = 7\,\text{TeV}$ collected between March and August 2011 with the ATLAS detector. Results are interpreted in a phenomenological minimal supersymmetric SM (pMSSM [20]) and in simplified models [21, 22]. In the pMSSM the masses of the $\tilde{\chi}_j^{\pm}$ and $\tilde{\chi}_i^0$ depend on the gaugino masses M_1 and M_2, the Higgs mass parameter $|\mu|$, and $\tan\beta$, the ratio of the expectation values of the two higgs doublets in the theory. The value of $\tan\beta$ has little impact on the phenomenology discussed here, and is fixed to 6, implying moderate mixing in the lepton sector. Gluon partners, squarks and left-handed sleptons are chosen to be heavy while the right-handed sleptons are assumed all to have $m_{\tilde{\ell}_R} = (m_{\tilde{\chi}_2^0} + m_{\tilde{\chi}_1^0})/2$. In these scenarios, decays to sleptons are favored. In the simplified models, the masses of the relevant particles (mass degenerate wino-like $\tilde{\chi}_1^{\pm}$ and $\tilde{\chi}_2^0$; bino-like $\tilde{\chi}_1^0$; $\tilde{\nu}$; $\tilde{\ell}_L$) are the only free parameters of the theory. The $\tilde{\chi}_1^{\pm}$ and $\tilde{\chi}_2^0$ are produced via the s-channel exchange of a virtual gauge boson and decay via left-handed sleptons and sneutrinos of mass $m_{\tilde{\nu}} = m_{\tilde{\ell}_L} = (m_{\tilde{\chi}_1^0} + m_{\tilde{\chi}_1^{\pm}})/2$) with a branching ratio of 50% to each.

2 Detector and Object Reconstruction

ATLAS [23] is a multipurpose particle physics detector with forward-backward symmetric cylindrical geometry. It consists of an inner tracker (ID) immersed in a 2 T magnetic field providing precision tracking of charged particles for pseudorapidities $|\eta| < 2.5$ [1]. A calorimeter system with either liquid argon (LAr) or scintillating tiles as the active media provides energy measurements over the range $|\eta| < 4.9$. The muon detector is installed on the barrel and endcap toroids and has trigger and high-precision tracking capabilities in the ranges $|\eta| < 2.4$ and $|\eta| < 2.7$, respectively.

Electron candidates are clustered energy deposits in the electromagnetic calorimeter matched to an ID track. They are required to have an associated cluster with $|\eta| < 2.47$ and transverse energy $E_{\text{T}} > 10\,\text{GeV}$, and to satisfy a tight set of identification criteria [24]. Muons are reconstructed by combining tracks in the ID and tracks in the muon spectrometer [25]. Reconstructed muons are considered as candidates

[1] ATLAS uses a right-handed coordinate system with its origin at the nominal interaction point (IP) in the centre of the detector and the z-axis along the beam pipe. The x-axis points from the IP to the centre of the LHC ring, and the y-axis points upward. Cylindrical coordinates (R, ϕ) are used in the transverse plane, ϕ being the azimuthal angle around the beam pipe. The pseudorapidity is defined in terms of the polar angle θ as $\eta = -\ln\tan(\theta/2)$.

if they have transverse momentum $p_{\mathrm{T}} > 10\,\mathrm{GeV}$, $|\eta| < 2.4$, and an impact parameter with respect to the primary vertex $|d_0| < 0.2\,\mathrm{mm}$. Electrons and muons well separated from each other and from candidate jets, for which a definition is given below, are referred to as "tagged" leptons. "Signal" leptons are tagged leptons for which the total transverse momentum within a $\Delta R \equiv \sqrt{(\Delta\phi)^2 + (\Delta\eta)^2} < 0.2$ around the lepton candidate is less than 10% of the E_{T} for electrons, and less than 1.8 GeV for muons. Jets are reconstructed from calibrated clustered energy deposits using the anti-k_t algorithm [26] with radius parameter of 0.4. The jet energy is corrected to account for the non-compensating nature of the calorimeter using correction factors obtained from Monte Carlo (MC) simulation and parameterized by jet η and E_{T} [27]. Jets used in this analysis have $E_{\mathrm{T}} > 20\,\mathrm{GeV}$ and $|\eta| < 2.8$. For a part of the data taking, a region in the second and third layer of the LAr barrel calorimeter became inactive causing an average 30% loss of the incident jet energy; events containing jets with $E_{\mathrm{T}} > 40\,\mathrm{GeV}$ in this area are rejected. Candidate electrons in the same region are removed. Jets are identified as containing a b-quark, and thus called "b-tagged", using information from the transverse impact parameter significance of the tracks and the expected topology of b- and c-quark decays. This algorithm [28] tags jets from b-quarks (light flavor quark or gluon) in top decays with an average efficiency of 60% ($< 1\%$) for jet $|\eta| < 2.5$ and jet $E_{\mathrm{T}} > 20\,\mathrm{GeV}$. The missing transverse momentum ($E_{\mathrm{T}}^{\mathrm{miss}}$) is the magnitude of the vector sum of the p_{T} of reconstructed objects in the event. Objects include muons (electrons) with p_{T} (E_{T}) above 10 GeV, jets with $E_{\mathrm{T}} > 20\,\mathrm{GeV}$, and calibrated calorimeter clusters with $|\eta| < 4.5$ not associated to these [29].

3 Monte Carlo Simulated Samples

Dedicated MC generators are used to simulate SM processes and SUSY signals relevant for this analysis. `HERWIG` [30] simulates diboson processes (WW, ZZ, WZ), while `MADGRAPH` [31] is used for $t\bar{t}V$ processes (where $V = Z, W$). `MC@NLO` [32] is adopted for the simulation of single and pair production of top quarks, while `ALPGEN` [33] is used to simulate V+jets. Expected diboson yields are normalized using next-to-leading (NLO) QCD predictions obtained with `MCFM` [34, 35]. The top pair production contribution is normalized to NNLO [36] while the ttV to NLO [37]. The QCD NNLO `Fewz` [38, 39] and `MCFM` cross sections are used for NNLO normalization of the Z and Zbb processes, respectively. The pMSSM and simplified model samples are produced with `HERWIG` and `MADGRAPH`, respectively, normalized to the NLO cross-sections obtained from `PROSPINO` [40] using the PDF set `CTEQ6.6` and with the renormalization/factorization scales set to the average of the gaugino masses in the process. Fragmentation and hadronization for the `ALPGEN` and `MC@NLO` (`MADGRAPH`) samples are performed with `HERWIG` (`Pythia` [41]). The choice of the parton density functions (PDFs) depends on the generator in question. `MRST 2007 LO`* [42] is used with `HERWIG`, `CTEQ6L1` [43] with `MADGRAPH` and `ALPGEN`, and `CTEQ6.6` [44] with `MC@NLO`. The propagation of the particles from the collision and the ATLAS detector is modeled using `GEANT4` [45]. The effect of multiple proton-proton collisions from the same or different bunch crossing is incorporated into the simulation by overlaying additional minimum bias events onto hard scatter events using `JIMMY` [46]. Simulated events are weighted to match the distribution of the mean number of interaction per bunch crossing observed in data.

4 Event Selection

The data sample was collected with a single muon (electron) trigger with a p_{T} (E_{T}) threshold of 18 GeV (20 or 22 GeV, depending on the instantaneous luminosity). At least one of the signal leptons is required to be within $\Delta R < 0.15$ of a trigger candidate lepton and have p_{T} (E_{T}) above 20 GeV (25 GeV) for muons (electrons). Events are considered for analysis if the ATLAS detector was running under nominal conditions, if at least one of the reconstructed primary vertices has four or more tracks associated to it

and if there are no jets with $|\eta| < 4.9$ failing the quality criteria described in [27]. Selected events must contain exactly three signal leptons. As leptonic decays of neutralinos yield same-flavor opposite-sign (SFOS) lepton pairs, the presence of at least one such pair is required. The invariant mass of any SFOS lepton pair must be above 20 GeV to suppress background from low mass resonances and the missing transverse momentum must satisfy $E_{\mathrm{T}}^{\mathrm{miss}} > 50\,\mathrm{GeV}$.

Two signal regions are then defined: a "Z-depleted" one (SR1), with no SFOS pairs with invariant mass within 10 GeV of the nominal Z-boson mass; and a "Z-enriched" one (SR2), where at least one SFOS pair gives an invariant mass in the same window. Events in SR1 are further required not to contain a b-tagged jet to suppress the backgrounds containing b-quarks. The SR1 (SR2) selection targets SUSY events with intermediate slepton (on-mass-shell Z-boson) decays.

5 Standard Model Backgrounds

Several SM processes contribute to the background in SR1 and SR2. A background process is considered "irreducible" if it leads to events with three real and isolated leptons, referred to as "real" leptons below. These include diboson (WZ and ZZ) and $t\bar{t}V$ production, where the gauge boson may be produced off-mass-shell. Their contribution is measured using the corresponding MC samples. A "reducible" process has at least one object, called "fake", which is either an electron or muon from semileptonic decays of heavy-flavor mesons, or an electron from an isolated photon. The contribution from misidentified light-flavor quark is negligible. The reducible background includes single- and pair-production of top-quarks, WW or V produced in association with jets or photons. The dominant component is due to semileptonic decays of top-quarks, with contribution of 1% or less from V production. This is estimated using a "matrix method" similar to that described in [47].

In this implementation of the matrix method, the signal lepton with the highest p_{T} or E_{T} is assumed to be real, which is valid in 99% of the cases based on MC studies. The number of events with one or two fakes is then extracted by solving a system of linear equations. Such a system establishes a relationship between the number of events in which the other two candidates are either signal or tagged leptons and those in which the candidates are either real or fake. The coefficients of the linear equations are functions of the real lepton identification efficiencies and of the fake object misidentification probabilities. Fake objects are classified by fake type (heavy flavor, conversion) and the corresponding misidentification probabilities are obtained from appropriate mixtures of MC samples. The identification efficiency is obtained in data for electrons and muons separately in events with a single SFOS lepton pair having invariant mass within 5 GeV of the Z mass. The misidentification probability is estimated for each process selecting events with one signal lepton and two tagged leptons. A weighted average of the misidentification probabilities is then computed by rescaling each simulated process in proportion to the corresponding cross-section. Correction factors depending on fake type are also applied in order to account for differences between values measured in data and in MC simulation. These factors are given by the ratio between the misidentification probability in data and that in MC simulation. For heavy flavor fakes, the correction is measured in $b\bar{b}$ events, while for fakes from photon conversions it is determined in a sample of photons radiated off a muon in $Z \to \mu\mu$ decays.

An additional source of background is due to virtual photons converting into muons for which an upper limit is obtained from data as follows. The number of observed events with exactly two signal leptons and $E_{\mathrm{T}}^{\mathrm{miss}} > 50\,\mathrm{GeV}$ is rescaled by the probability that any of the signal leptons could have radiated the converted photon. The probability is measured in events with $E_{\mathrm{T}}^{\mathrm{miss}} < 50\,\mathrm{GeV}$ as the ratio of number of events with three signal muons to that with two signal muons, giving a dilepton or trilepton invariant mass within 10 GeV of the nominal Z boson mass.

The background predictions have been validated in a control region dominated by Z/γ^* production (VR1: 3 signal leptons, $30 < E_{\mathrm{T}}^{\mathrm{miss}} < 50\,\mathrm{GeV}$) and in one dominated by $t\bar{t}$ (VR2: 3 signal leptons, SFOS

lepton pairs vetoed, $E_{\mathrm{T}}^{\mathrm{miss}} > 50\,\mathrm{GeV}$). Data and predictions are in agreement within the quoted statistical and systematic uncertainties as shown in Table 1.

6 Systematic Uncertainties

In SR1, the primary source of systematic uncertainty on the background is that on the reducible component (17%). This originates from the uncertainty on the weighted average misidentification probability as a consequence of the cross-section scale and PDF dependence (10–30%), of the dependence of the misidentification probability on $E_{\mathrm{T}}^{\mathrm{miss}}$ (0.4–17%), and of the data-to-MC correction factors (10–50%). For the irreducible background we assume a theoretical uncertainty on the Monte Carlo simulation of 20–25% . An additional 10% is due to the limited number of simulated events . Other uncertainties, such as jet energy scale and resolution, lepton energy scale and resolution, lepton efficiency, b-tagging efficiency, event quality selection, range between 0.2–5%. A 3.7% [48] uncertainty on the luminosity is also taken into account. In SR2, uncertainties are similar to those in SR1, except for a smaller uncertainty (4%) due to the simulated sample statistics. Theoretical systematic uncertainties on the `PROSPINO` cross-sections are evaluated by increasing and decreasing the renormalization and factorization scales by a factor of two. The uncertainty on α_S and the maximum uncertainty between the `CTEQ6.6` and `MSTW` [49] set are also included. The resulting signal uncertainties are in the 10–15% range, also including contributions from all experimental sources considered for the irreducible background.

7 Results

The numbers of observed events and the prediction for SM backgrounds in SR1 and SR2 are reported in Table 1. The probability that the background fluctuates to the observed number of events or higher is calculated in the frequentist approach and found to be 19% (10%) in SR1 (SR2). The distributions of the $E_{\mathrm{T}}^{\mathrm{miss}}$ in the two signal regions are presented in Fig. 1. The yield for one of the simplified model scenarios ($m_{\tilde{\chi}_1^\pm}, m_{\tilde{\chi}_2^0}, m_{\tilde{\ell}_L}, m_{\tilde{\chi}_1^0} = 150$, 150, 100, 50 GeV) is also shown in SR1 for illustration purposes.

Table 1: Expected number of events from SM backgrounds (Bkg. in the table) and observed number of events in data, for 2.06 fb^{-1}, in control regions VR1 and VR2, and in signal regions SR1 and SR2. Both statistical and systematic uncertainties are included.

Selection	VR1	VR2	SR1	SR2
$t\bar{t}V$	1.4±0.6	0.7±0.6	0.4±0.3	2.7±2.1
ZZ	6.7±1.8	0.03±0.04	0.7±0.2	3.4±0.9
WZ	61±15	0.4±0.2	11±3	58±14
Reducible Bkg.	56±35	14±9	14±4	7.5±3.9
Total Bkg.	125±38	15±9	26±5	72±15
Data	122	12	32	95

No significant excess of events is found in either signal region. An upper limit on the visible production cross-section of 10.0 fb (26.1 fb) in SR1 (SR2) is placed at 95% confidence level (CL) with the modified frequentist CL$_s$ prescription [50]. The corresponding expected limits are 7.3 fb and 16.7 fb. All systematic uncertainties and their correlations are taken into account via nuisance parameters. The limits are interpreted in the pMSSM with $M_1 = 100$ GeV and the simplified models for SR1, providing the best sensitivity over the entire mass plane (Fig. 2). The acceptance for $M_1 = 100$ GeV is higher than for larger values of M_1 due to the sizable mass splitting between $\tilde{\chi}_1^\pm$ and $\tilde{\chi}_1^0$. In the simplified models degenerate

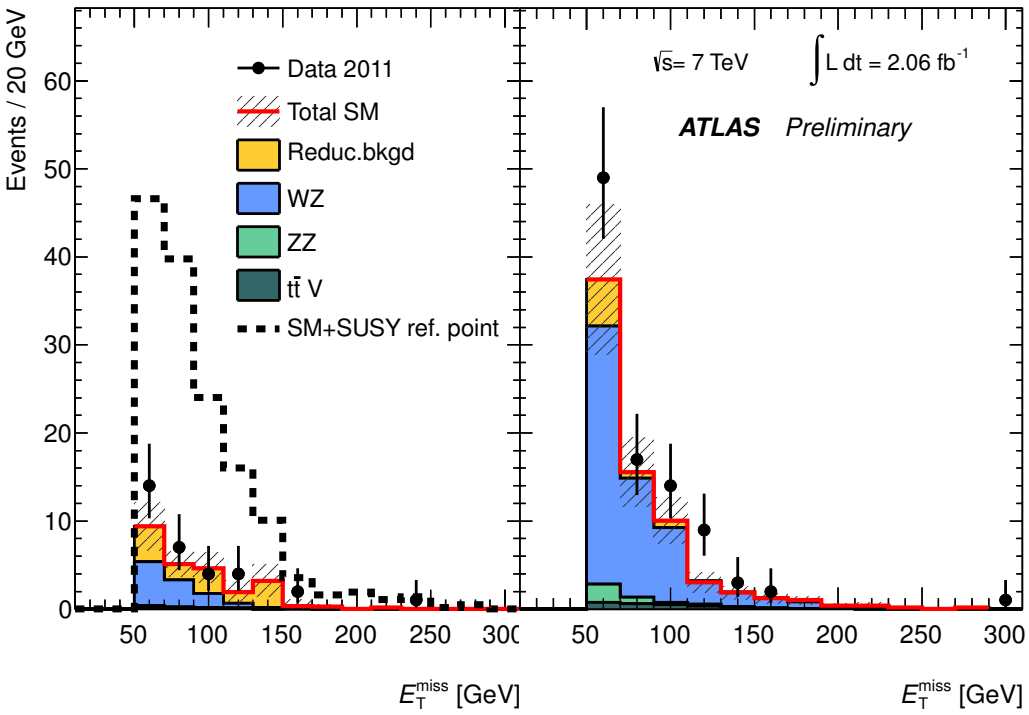

Figure 1: $E_{\mathrm{T}}^{\mathrm{miss}}$ distributions for events in signal regions SR1 (left) and SR2 (right). The error band includes both statistical and systematic uncertainty, while the errors on the data points are statistical only. The SUSY reference point used in SR1 is the simplified model scenario with $m_{\tilde{\chi}_1^\pm}, m_{\tilde{\chi}_2^0}, m_{\tilde{\ell}_L}, m_{\tilde{\chi}_1^0} = 150$, 150, 100, 50 GeV.

$\tilde{\chi}_1^\pm$ and $\tilde{\chi}_2^0$ masses up to 300 GeV are excluded for large mass differences to the $\tilde{\chi}_1^0$. Care has to be taken when interpreting the simplified model limit in the context of a pMSSM scenario, where in general the the mass of the sneutrino is lighter than the mass of the left-handed slepton, leading to higher lepton momenta from chargino decays but also to a change in the branching ratios of the $\tilde{\chi}_2^0$.

8 Conclusions

In summary, results from a search for charginos and neutralinos in the three lepton and missing transverse momentum final states are reported. The analysis is based on 2.06 fb^{-1} of 7 TeV proton-proton collision data delivered by the LHC and recorded with the ATLAS detector in 2011. No significant excess of events is found in data. The null result is interpreted in pMSSM and in simplified models. For the simplified models, degenerate lightest chargino and next-to-lightest neutralino masses are excluded up to 300 GeV for mass differences to the lightest neutralino up to 250 GeV.

References

[1] H. Miyazawa Prog. Theor. Phys. **36 (6)** (1966) 1266.

[2] P. Ramond Phys. Rev. **D3** (1971) 2415.

[3] Y. Golfand, E. Likhtman JETP Lett. **13** (1971) 323.

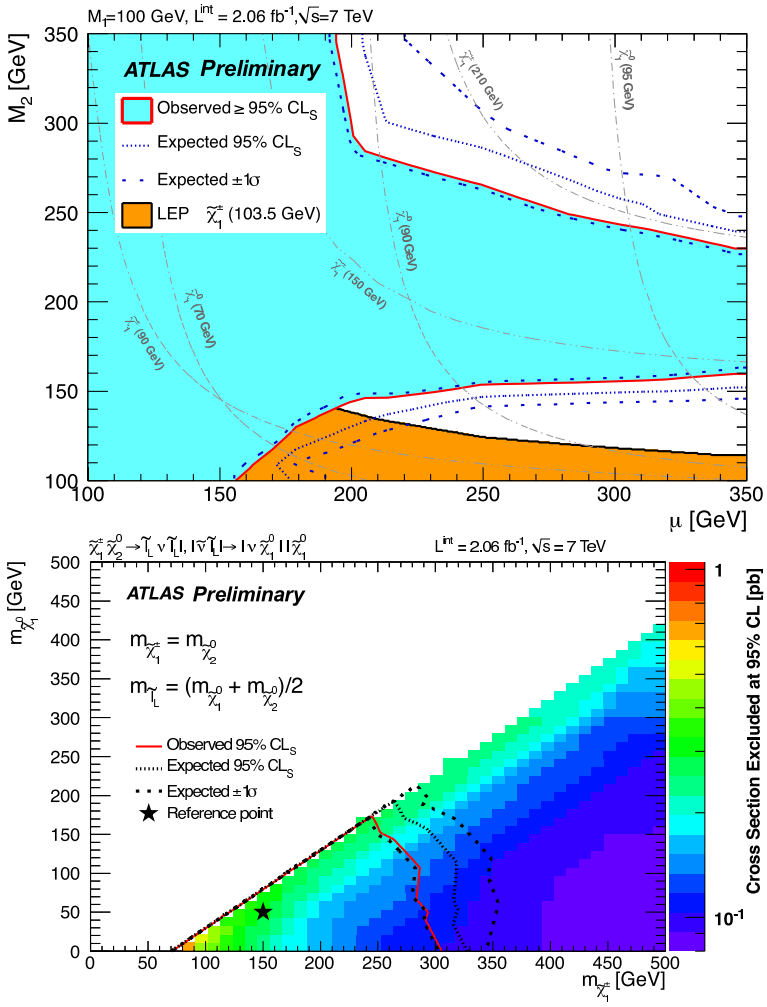

Figure 2: Observed and expected 95% CL limit contours for chargino and neutralino production in the pMSSM (upper) and simplified model (lower) scenarios. For the simplified models, the 95% CL upper limit on the production cross-section is also shown. Interpolation is used to account for the discreteness of the signal grids.

[4] A. Neveu and J. H. Schwarz Nucl. Phys. **B31** (1971) 86.

[5] A. Neveu and J. H. Schwarz Phys. Rev. **D4** (1971) 1109.

[6] J. Gervais and B. Sakita Nucl. Phys. **B34** (1971) 632.

[7] D. Volkov and V. Akulov Phys. Lett. **B46** (1973) 109.

[8] J. Wess and B. Zumino Phys. Lett. **B49** (1974) 52.

[9] J. Wess and B. Zumino Nucl. Phys. **B70** (1974) 39.

[10] P. Fayet Phys. Lett. **B64** (1976) 159.

[11] P. Fayet Phys. Lett. **B69** (1977) 489.

[12] G. R. Farrar and P. Fayet Phys. Lett. **B76** (1978) 575.

[13] P. Fayet Phys. Lett. **B84** (1979) 416.

[14] S. Dimopoulos and H. Georgi Nucl. Phys. **B193** (1981) 150.

[15] Tech. Rep. LHWG-note-2001-05, CERN, Geneva, July, 2001.

[16] D0 Collaboration, V. Abazov et al. Phys. Lett. **B680** (2009) 34.

[17] CDF Collaboration, T. Aaltonen et al. Phys. Rev. Lett. **101** (2008) 251801.

[18] ATLAS Collaboration. Submitted to Phys. Lett. B, arXiv:1110.6189, 2011.

[19] CMS Collaboration. SUS-11-013-PAS, 2011.

[20] A. Djouadi, J.L. Kneur, G. Moultaka Comput. Phys. Commun. **176** (2007) 426.

[21] J. Alwall, P. Schuster, N. Toro Phys. Rev. **D79** (2009) 075020.

[22] D. Alves et al. arXiv:1105.2838, 2011.

[23] ATLAS Collaboration JINST **3** (2008) S08003.

[24] ATLAS Collaboration. Submitted to Eur. Phys. J. C, arXiv:1110.3174, 2010.

[25] ATLAS Collaboration, JHEP **12** (2010) 60.

[26] M. Cacciari, G.P. Salam, G. Soyez JHEP **04** (2008) 063.

[27] ATLAS Collaboration. submitted to Eur. Phys. J. C, arXiv:1112.6426, 2011.

[28] ATLAS Collaboration. ATLAS-CONF-2011-102, https://cdsweb.cern.ch/record/1369219, 2011.

[29] ATLAS Collaboration Eur. Phys. J. **C72** (2012) 1844.

[30] G. Corcella et al. JHEP **0101** (2001) 010.

[31] J. Alwall, M. Herquet, F. Maltoni, O. Mattelaer, T. Stelzer JHEP **06** (2011) 128.

[32] S. Frixione and B.R. Webber JHEP **0206** (2002) 029.

[33] M. Mangano et al. JHEP **0307** (2003) 001.

[34] R. K. E. J. M. Campbell Phys. Rev. D **60** (1999) 113006.

[35] C. W. J. M. Campbell, R. K. Ellis JHEP **07** (2011) 018.

[36] M. Aliev, et al. Comput. Phys. Commun. **182** (2011) 1034.

[37] A. Kardos et al. arXiv:1111.0610, 2011.

[38] F. P. K. Melnikov Phys. Rev. D **74** (2006) 114017.

[39] C. Anastasiou et al. Phys. Rev. D **69** (2004) 094008.

[40] W. Beenakker et al. Nucl. Phys. **B492** (1997) 51.

[41] T. Sjostrand, S. Mrenna, P. Skands JHEP **05** (2006) 026.

[42] A. Sherstnev, R. Thorne Eur. Phys. J. **C55** (2008) 553.

[43] J. Pumplin et al. J. High Energy Phys. **0207** (012) 2002.

[44] P. M. Nadolsky et al Phy. Rev. **D78** (2008) 013004.

[45] GEANT4 Collaboration Nucl. Instrum. Meth. **A506** (2003) 250–303.

[46] J.M. Butterworth, J.R. Forshaw, M.H. Syemour Z. Phys. **C72** (1996) 637.

[47] ATLAS Collaboration Eur. Phys. J. **C71** (2011) 1577.

[48] ATLAS Collaboration Eur. Phys. J. **C71** (2011) 1630.

[49] A. Sherstnev, R. S. Thorne Eur. Phys. J. **C55** (2008) 553575.

[50] A. L. Read J. Phys. **G28** (2002) 2693.

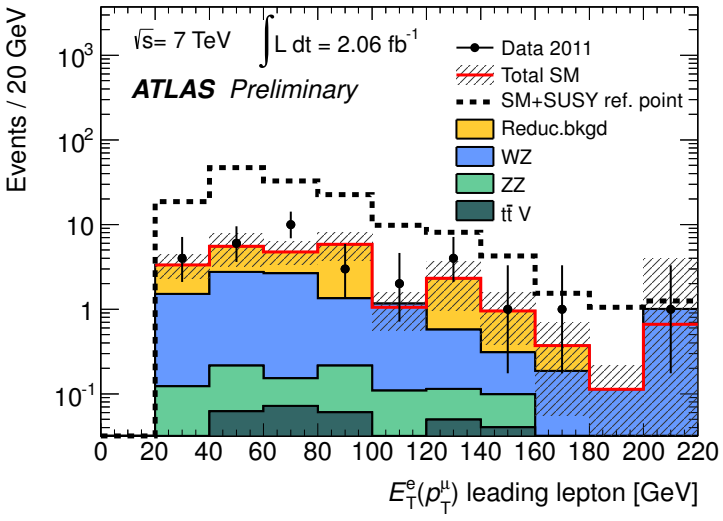

Figure 3: p_{T} distribution of the first leading lepton for events in SR1 for data and SM predictions. The grey band represents statistical and systematic uncertainties added in quadrature. The SUSY reference point is the simplified model scenario with $m_{\tilde{\chi}_1^\pm}, m_{\tilde{\chi}_2^0}, m_{\tilde{\ell}_L}, m_{\tilde{\chi}_1^0} = 150, 150, 100, 50\,\mathrm{GeV}$.

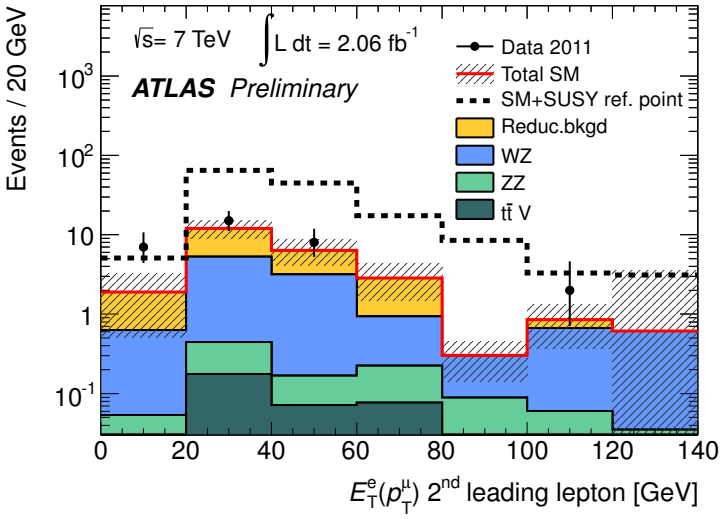

Figure 4: p_{T} distribution of the second leading lepton for events in SR1 for data and SM predictions. The grey band represents statistical and systematic uncertainties added in quadrature. The SUSY reference point is the simplified model scenario with $m_{\tilde{\chi}_1^\pm}, m_{\tilde{\chi}_2^0}, m_{\tilde{\ell}_L}, m_{\tilde{\chi}_1^0} = 150, 150, 100, 50\,\mathrm{GeV}$.

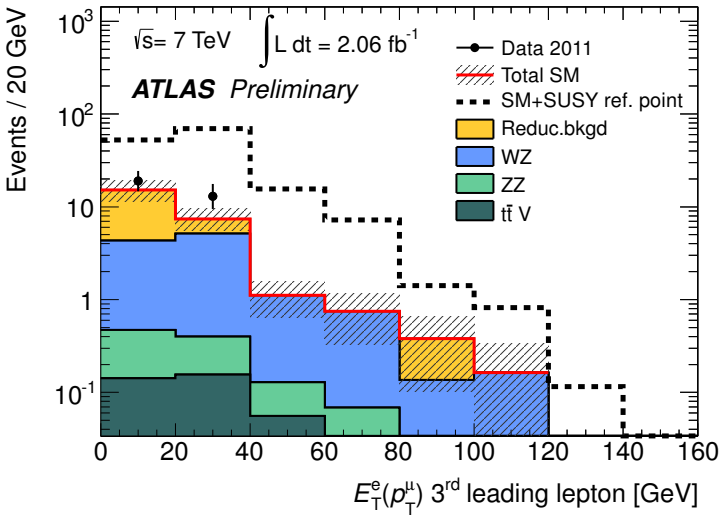

Figure 5: p_{T} distribution of the third leading lepton for events in SR1 for data and SM predictions. The grey band represents statistical and systematic uncertainties added in quadrature. The SUSY reference point is the simplified model scenario with $m_{\tilde{\chi}_1^\pm}, m_{\tilde{\chi}_2^0}, m_{\tilde{\ell}_L}, m_{\tilde{\chi}_1^0} = 150, 150, 100, 50\,\mathrm{GeV}$.

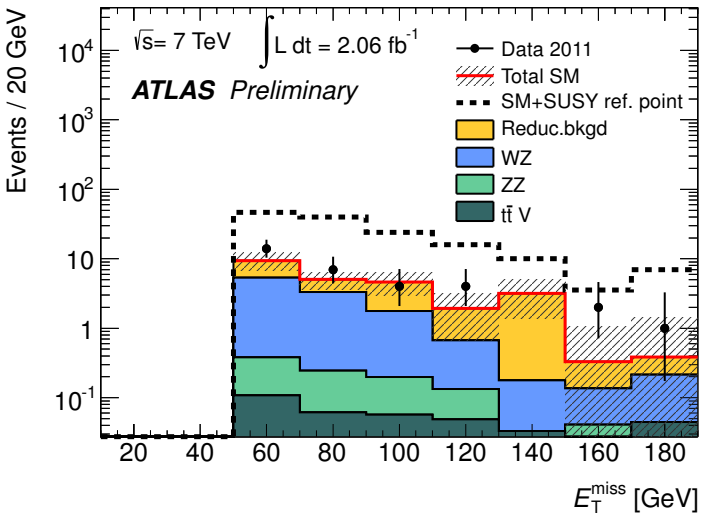

Figure 6: $E_{\mathrm{T}}^{\mathrm{miss}}$ distribution for events in SR1 for data and SM predictions. The grey band represents statistical and systematic uncertainties added in quadrature. The SUSY reference point is the simplified model scenario with $m_{\tilde{\chi}_1^\pm}, m_{\tilde{\chi}_2^0}, m_{\tilde{\ell}_L}, m_{\tilde{\chi}_1^0} = 150, 150, 100, 50\,\mathrm{GeV}$.

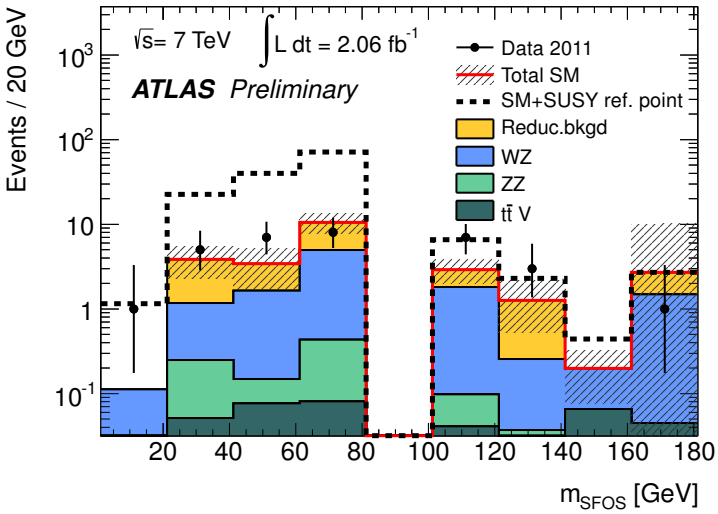

Figure 7: Invariant mass m_{SFOS} of the same-flavor-opposite-sign (SFOS) lepton pair for events in SR1 for data and SM predictions. In events where multiple SFOS lepton pairs are present, the pair with invariant mass closest to the Z boson mass is plotted. The grey band represents statistical and systematic uncertainties added in quadrature. The SUSY reference point is the simplified model scenario with $m_{\tilde{\chi}_1^\pm}, m_{\tilde{\chi}_2^0}, m_{\tilde{\ell}_L}, m_{\tilde{\chi}_1^0} = 150, 150, 100, 50\,\mathrm{GeV}$.

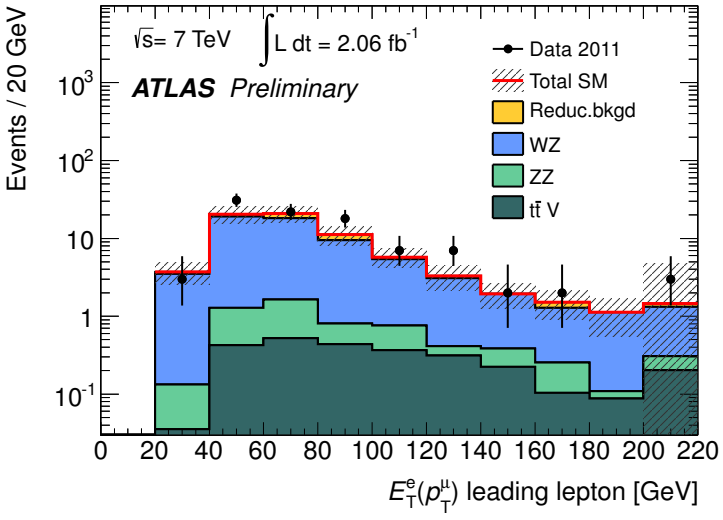

Figure 8: p_{T} distribution of the first leading lepton for events in SR2 for data and SM predictions. The grey band represents statistical and systematic uncertainties added in quadrature.

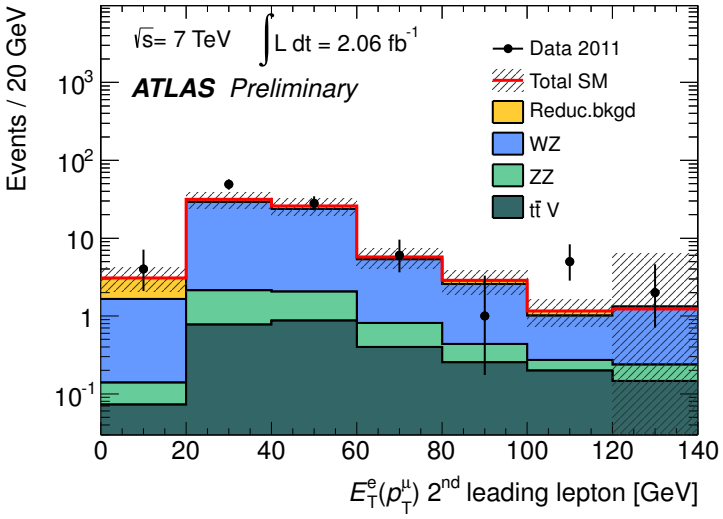

Figure 9: p_{T} distribution of the second leading lepton for events in SR2 for data and SM predictions. The grey band represents statistical and systematic uncertainties added in quadrature.

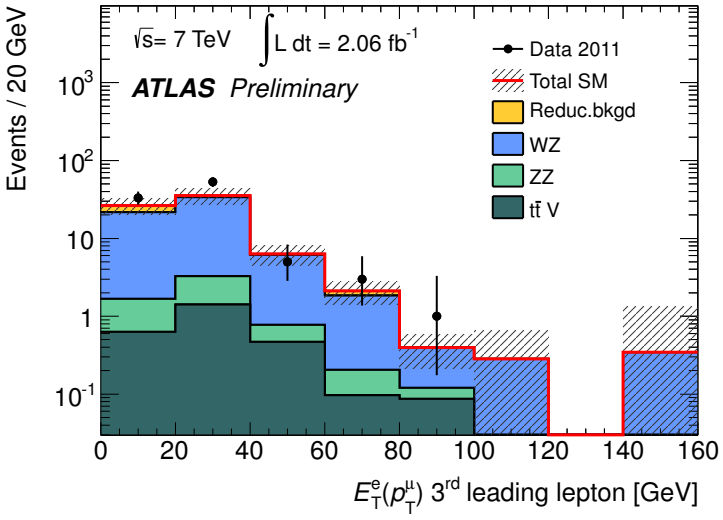

Figure 10: p_{T} distribution of the third leading lepton for events in SR2 for data and SM predictions. The grey band represents statistical and systematic uncertainties added in quadrature.

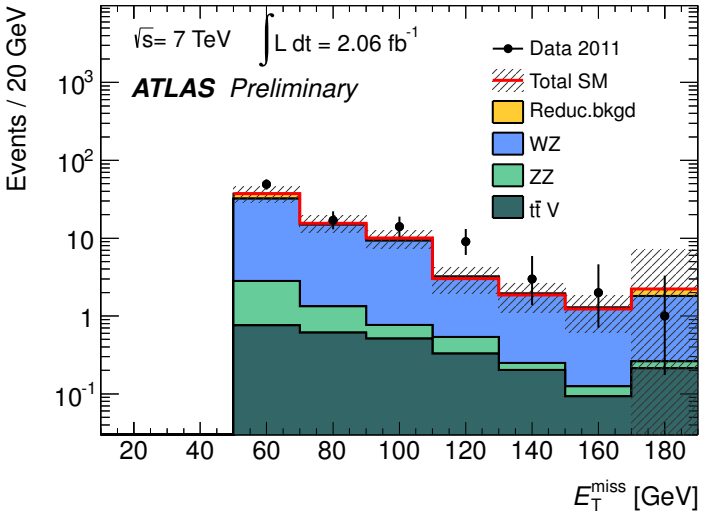

Figure 11: $E_{\mathrm{T}}^{\mathrm{miss}}$ distribution for events in SR2 for data and SM predictions. The grey band represents statistical and systematic uncertainties added in quadrature.